JOURNAL OF Materials CHEMISTRY

Following the structural changes in iron phosphate catalysts by *in situ* combined XRD/QuEXAFS technique

Andrew M. Beale and Gopinathan Sankar*

Davy Faraday Research Laboratory, The Royal Institution of GB, 21 Albemarle Street, London, UK W1S 4BS

Received 29th April 2002, Accepted 14th June 2002
First published as an Advance Article on the web 2nd August 2002

The structure of iron phosphate catalysts prepared by three different synthetic methods has been studied using *in situ* combined XRD/QuEXAFS. Two of the synthesis procedures have previously been employed to produce these catalysts whilst the third is a new method employing hydrothermal techniques. The combined XRD/QuEXAFS approach supported by *ex situ* measurements carried out using XRD, TGA and surface area measurements, showed that all three methods produced a catalyst precursor material, having the chemical composition of $FePO_4{\cdot}2H_2O$. The *in situ* study clearly shows the loss of two water molecules during the initial stages of heating and a transformation to $FePO_4$ having tridymite type structure takes place at temperatures above *ca.* 100 °C. The crystallinity of the tridymite phase appeared to improve upon heating to *ca.* 500 °C and above which a further transformation to a quartz phase takes place. Of the three catalysts, the material produced by hydrothermal methods was found to be the most phase pure and to possess a higher surface area than the materials prepared by the other two methods.

Introduction

Iron phosphates have been identified as excellent catalysts for oxidative dehydrogenation reactions.[1,2] They are known to be particularly active for the selective conversion of isobutyric acid to methacrylic acid, which can be easily esterified to produce methyl methacrylate, an important intermediate in a large number of chemical processes. Use of this solid catalyst removes some of the problems encountered, in particular the formation of unwanted by-products and disposal of waste products, when other catalysts such as sulfuric acid are used. Since the first patent for the preparation and reaction of an iron phosphate catalyst was published in 1971,[3] several research articles and patents have appeared in the literature, which have been summarised in a recent review.[2] In particular, it has been noted that the catalytic performance is related to the method of preparation.[4] In general, the starting iron phosphate material has been prepared mainly by co-precipitation methods in which appropriate amounts of a ferric compound, such as ferric nitrate were dissolved in water, and to this solution phosphoric acid was added before the mixture was heated and dried to yield the starting material.[2] A variation on this theme is the ammonia gel method first used by Ai and Ohdan.[5] Here the preparation involved the reaction of ferric nitrate solution with dilute ammonia to form an iron hydroxide gel, which was subsequently reacted with phosphoric acid before the mixture was heated and dried at *ca.* 100 °C. The final dried pastes obtained by these methods were then calcined at temperatures between 400 °C and 600 °C before being used for catalytic reaction. As mentioned previously most of the synthesis procedures reported are variations of the co-precipitation technique. However, catalysts have been successfully synthesised using other methods such as the 'Vivianite method' reported by Bonnet *et al.*[6] which utilises the mineral Vivianite ($Fe_3(PO_4)_2{\cdot}8H_2O$) and $H_4P_2O_7$ refluxed in acetone. Many studies have reported that the method of preparation, calcination temperature and stoichiometry can affect catalytic performance.[4,5,7,8] In particular, it has been noted that the most active catalysts have a P : Fe ratio of 1.2 in the starting material.[4] But although stoichiometry has been shown to play an important role, in addition to the overall crystal structure of the catalyst, a general conclusion is that the charge-state of iron (including a possible Fe^{3+}/Fe^{2+} redox couple) is critical to the catalytic mechanism (*via* a Mars and Van Krevelen type mechanism) and performance.[9–11] Although some structural studies have been undertaken on both the calcined materials and the catalysts after subjecting to a catalytic reaction,[5,12] to our knowledge there hasn't been any attempt to characterise the starting material or to determine the phase formation during the calcination process. Here we report a detailed *in situ* study of the catalysts prepared by two popular methods and in addition, we have discovered during the course of this study, a new efficient and simpler method of preparing the catalyst precursor by employing hydrothermal methods normally employed for the synthesis of microporous materials. In addition, for certain applications, the hydrothermal synthesis procedure is also used for the preparation of oxides and sulfides.[13–17]

In order to follow the formation of the active catalyst from the precursor material, we have used X-ray absorption spectroscopy (XAS) and X-ray diffraction techniques (XRD).[18] While the latter is commonly used in the study of crystalline solids, the former technique is widely employed in the study of crystalline or amorphous materials. The main reason being, X-ray absorption spectroscopy which consists of X-ray absorption near edge structure (XANES) and extended absorption fine structure (EXAFS), is not only atom-specific but also does not depend on long-range order. It has been shown for a variety of systems that XANES can be used effectively to determine both the oxidation-state and the local environment of the absorbing species.[19–21] When used in conjunction with EXAFS (from which a more detailed local structural arrangement can be elucidated), the two methods can be effectively used to determine the structure of active sites. Combining this with the X-ray diffraction measurements makes it a much more powerful technique, which is capable of delivering structural details at the atomic level.[22–25] By using a powerful X-ray source, such as synchrotron radiation, and more importantly the ability of measuring high-quality XAS data in few minutes (which is called QuEXAFS, an acronym we will use in this paper for X-ray absorption spectroscopy), it is now routinely possible to track the structural changes that occur during catalyst synthesis, activation and, more importantly, reactions.[18,23–25]

 DOI: 10.1039/b204059j

This *in situ* combined XRD/QuEXAFS method has been used effectively in the study of many microporous metal ion substituted aluminophosphates, solid state oxide catalysts and a variety of other systems.[24–32] The present *in situ* combined XRD/QuEXAFS study of iron phosphate catalysts prepared by three different methods clearly showed a change in iron coordination from octahedral to tetrahedral occurs during the initial stages of the heat treatment process. Subsequent formation of a tridymite phase takes place before the transformation to quartz phase at temperatures above 500 °C. TGA and mass spectrometry measurements have also been performed on these materials to support the findings observed by the *in situ* combined XRD/QuEXAFS study. The catalytic tests performed by the catalyst prepared by hydrothermal procedures indicate that the overall performance is better than that prepared using conventional procedures.

Experimental

The details of the preparation of the iron phosphate catalyst precursors prepared by three different methods are given below.

Precipitation method

We followed procedures similar to the one described in the literature.[2] In a typical synthesis, 6.1 g of iron nitrate was dissolved in 100 ml of water. Orthophosphoric acid was slowly added to this solution and the mixture was stirred for four hours at *ca.* 100 °C. The final paste (white in colour) was dried for six hours at 100 °C.

Ammonia-gel method

Once again, we followed the procedures given in the literature.[5] In a typical synthesis, 6.1 g of iron nitrate was reacted with ammonium hydroxide to form a gel. The gel was filtered and washed before reacting with appropriate amounts of orthophosphoric acid. This mixture was then stirred and heated for four hours before the excess water was removed. The resultant catalyst precursor paste (white in colour) was dried for six hours at 100 °C.

Hydrothermal method

In this new procedure, iron hydroxide was used as prepared in the ammonia gel method. The resulting gel was dissolved in orthophosphoric acid before the mixture was subjected to hydrothermal treatment in a Teflon lined autoclave, at 175 °C for four hours. The autoclave was cooled and the contents (a white powder) were washed and dried at 100 °C.

XRD patterns of all the as-synthesised materials (dried at 100 °C) were recorded using FR571 Enraf-Nonius diffractometer (of Bragg–Brentano geometry) equipped with a copper target. TGA measurements were carried out using a Shimadzu TGA 50 with the samples heated in air over a temperature range of 25 –600 °C. The BET surface area measurements were carried out on both the as-prepared and on the catalysts calcined at 400 °C and 600 °C employing a Micromeritics Gemini III. All samples were subjected to degassing at 100 °C in N_2 prior to surface area measurement using N_2 at −196 °C as the absorbent. The error in the determination of the surface area is estimated to be *ca.* ± 2 m^2 g^{-1}. Online mass spectrometry experiments were carried out using a VG quadrupole mass spectrometer to monitor the gaseous decomposition products that evolve during the calcination of the as-prepared catalyst at 600 °C in air.

In situ XRD/QuEXAFS measurements were carried out at station 9.3 of the Daresbury Synchrotron radiation source, which operates at 2 GeV with a typical current of 150 to 250 mA. The station was equipped with a Si(111) double crystal monochromator, and ion chambers for measuring incident and transmitted beam intensities for recording X-ray absorption spectra. For diffraction measurements, a position sensitive INEL detector was used. In a typical experiment, about 40 mg of the precursor iron phosphate material was pressed into a disc of 13 mm diameter. This sample was placed into an *in situ* cell that permits the measurement of combined XAS and XRD data. The samples were heated at 5 °C min^{-1} from room temperature to 400 °C and held at this temperature for 30 minutes before heating further to 600 °C. Fe K-edge XAS and XRD data were collected sequentially during this activation process. The time taken to collect the Fe K-edge XAS pattern was 380 s and 180 s for the XRD data resulting in a total cycle time of 10 minutes, which included 40 s dead time to move the monochromator back to the starting point. XRD data were collected at a wavelength of 1.775.Å, well below the Fe K-edge absorption to avoid fluorescence effects. The INEL detector was calibrated using a NBS silicon standard and a 10 μm Fe foil was used to calibrate the monochromator position.

Phosphorus K-edge data were collected on station 3.4 of the Daresbury Synchrotron radiation source. The station was equipped with an InSb double crystal monochromator with an ion chamber for measuring incident radiation and a Canbera fluorescence detector. Typically a few milligrams of sample was mixed with graphite and mounted onto a sample mount which was placed into the experimental chamber before measurements were carried out under vacuum.

XAS data were processed using the suite of programs available at Daresbury laboratory, namely EXCALIB (for converting the raw data to energy *vs.* absorption coefficient), EXBROOK (to obtain normalised XANES part of the spectra and for background subtraction to extract EXAFS) and EXCURV98 (to perform detailed refinement using multiple scattering procedures to extract more detailed local structural details of the catalysts).

Results and discussion

First we discuss the structure of the as-synthesised catalyst, subsequently we show the *in situ* combined XRD/QuEXAFS results, which allowed us to follow the changes that took place during the calcination process, and finally we discuss the structure of calcined catalyst.

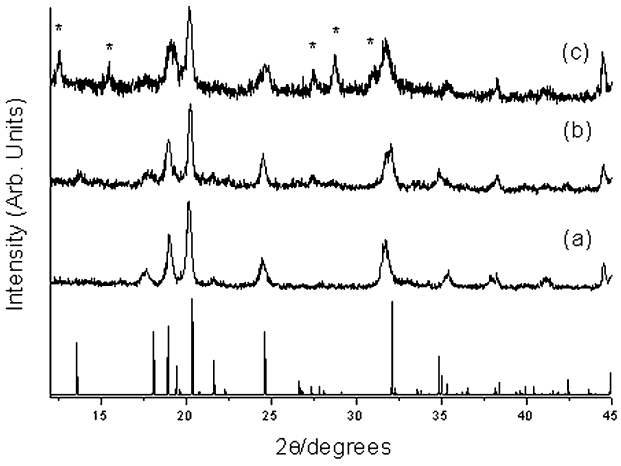

Fig. 1 XRD patterns of (a) an iron phosphate catalyst prepared by the hydrothermal method, (b) an iron phosphate catalyst prepared by the precipitation method and (c) an iron phosphate catalyst prepared by the ammonia gel method. Reflections that are not related to the $FePO_4 \cdot 2H_2O$ phase are asterisked, and correspond to an unidentifiable minority phase. The lines mark the 2θ positions at which the reflections corresponding to the mineral phase metastrengite appears.

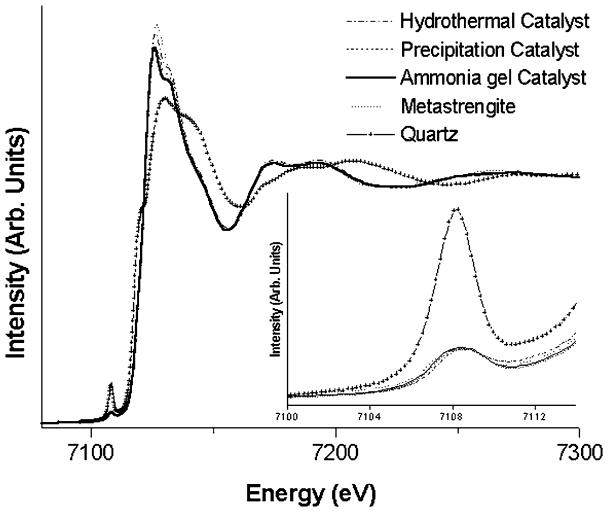

Fig. 2 Fe K-edge XANES of the as-prepared iron phosphate materials, employing various procedures. Fe K-edge XANES of the as-synthesised $FePO_4{\cdot}2H_2O$ material having a metastrengite structure and the quartz form of $FePO_4$, in which the Fe(III) ions are present in octahedral and tetrahedral environments, are also given for comparison. The in set shows the pre-edge part of the spectra for clarity.

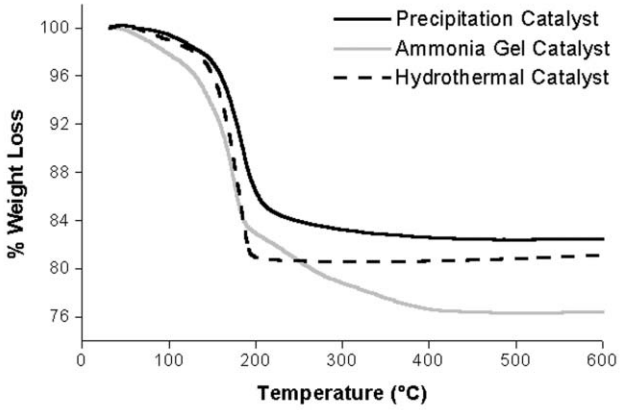

Fig. 3 Thermogravimetric measurements of the iron phosphate catalysts prepared by the three different methods.

As-prepared catalysts

In Fig. 1 we show the X-ray diffraction patterns of the as-prepared catalysts synthesised by the three methods. The XRD patterns of the as-synthesized catalysts are very similar to the one reported in the literature for the $FePO_4{\cdot}2H_2O$ type phase.[33,34] Although some of the reflections of the iron phosphate materials prepared by us coincide with the well-known iron phosphate mineral, metastrengite ($FePO_4{\cdot}2H_2O$), it appears from direct comparison that these as-synthesised solids are not the same as the mineral form. The extra reflections (asterisked in Fig. 1) seen in the ammonia gel catalyst suggest that an additional unidentified phase(s) co-exists along with the $FePO_4{\cdot}2H_2O$ type phase. In Fig. 2 we show a comparison plot, concentrating on the pre-edge peak (see inset in Fig. 2) of the Fe K-edge XANES for each of the as-prepared materials and for two model iron phosphate compounds ($FePO_4$ and metastrengite $FePO_4{\cdot}2H_2O$) known to contain tetrahedral and octahedral Fe^{3+} respectively. It is well known that pre-edge intensity is sensitive to the local coordination geometry with a non-centrosymmetric tetrahedral environment showing a higher intensity than an octahedral or a distorted geometry.[21,22,35,36] Although this pre-edge intensity, which is due to a 1s⟶3d transition, is dipole forbidden, it has been interpreted as being due to the mixing of p orbitals of both the ligand and the 4p state of the cation allowing this transition to take place. It was also shown that the intensity of the transition not only depended on the coordination geometry but also on the metal–oxygen distances.[37,38] Thus a combination of these effects, which are due to the change in coordination geometry, can give rise to a higher pre-edge intensity for a tetrahedrally coordinated system compared to an octahedral one. It is clear from Fig. 2 that the spectra of all of the as-prepared catalysts are very similar to metastrengite ($FePO_4{\cdot}2H_2O$), which suggests that the as-prepared catalysts contain predominantly octahedral Fe^{3+} ions. However, although all of the as-prepared catalysts have a similar octahedral environment to that of metastrengite ($FePO_4{\cdot}2H_2O$), it is difficult to determine whether water molecules contribute to the formation of this octahedral geometry in all of the as-prepared catalysts. In order to determine the nature of various loosely bound species present in the catalyst, first we carried out a thermogravimetric analysis (TGA) of all the catalysts.

Fig. 3 shows the TGA data recorded for all three catalysts. For each of the catalysts major weight loss was observed between 100 and 200 °C. Beyond this temperature only the ammonia gel sample shows further weight loss. The percentage weight loss observed for all three catalysts at temperatures below 200 °C corresponds to approximately 20 percent of the starting mass and can be explained as the loss of two water molecules from a $FePO_4{\cdot}2H_2O$ type species. Independent online mass spectrometry experiments confirmed the loss of water molecules from all the three catalysts on heating up to *ca.* 200 °C. The continued reduction in mass at higher temperatures observed for the catalyst prepared by the ammonia gel method may be associated with the loss of ammonia ligands present in an additional phase. Ai *et al.*[4] observed similar behaviour in a previous investigation.

Having established the presence of octahedral coordination from the XANES and the presence of two water molecules by TGA, we analysed the EXAFS data of the as-prepared catalysts using multiple scattering (MS) procedures. Models were constructed using the reported structures for metastrengite. In this MS method all the oxygen and phosphorous atoms were considered as individual shells resulting in a set of neighbours containing six oxygen and four phosphorous atoms. Among the six oxygens attached to the iron center, four were treated as bridging oxygens linking the iron and phosphorous atoms and the other two as being part of two water molecules. Because of the complexity of the model, it was necessary to treat them as C_1 symmetry for MS calculations. In order to avoid the refinement of too many independent parameters a set of constraints and restraints were imposed, taking chemical knowledge into account. For example, all the Fe–O distances and Debye–Waller factors were constrained to be the same value, since they are likely to be very similar. However, in the case of Fe–P distances, they should not be taken as the same values, since the bond-angles are likely to be different and hence they may have different MS effects. Thus the refinement of the Fe–P shells and the Fe–O–P bond angles were carried out independently; with the Fe–P Debye–Waller factor all of the shells constrained to be the same. The refinement was performed by restraining the O–P distances to be *ca.* 1.532 Å, obtained from the analysis of the P K-edge data (see Table 1 and Fig. 4(a) and 4(b)); P K-edge data were analysed using a simple single scattering approximation due to a limited data range. Similar MS procedures have been used successfully by us in determining the structure of transition metal ions in a framework of substituted microporous solids.[39] The final refinement yielded the local structure of the Fe^{3+} centre for the hydrothermally prepared catalyst and the resulting structural parameters are given in Table 1. The best fit between experimental Fe K-edge EXAFS data and the calculated EXAFS using parameters in Table 1

Table 1 Structural parameters obtained from the EXAFS data of the as-prepared iron phosphate material, synthesised using hydrothermal methods

K-Edge	Atom pair	*N*	*R*/Å	$2\sigma^2$/Å^2	Fe–O–P angle/°	*R* Factor
P	P–O	3.72	1.532	0.0061		35.61
Fe	Fe–O_w[a]	2	2.02	0.022		
	Fe–O_b[b]	4	1.95	0.013		
	Fe–P10	1	3.42	0.018	157	20.08
	Fe–P7	1	3.32	0.018	164	
	Fe–P9	1	3.32	0.018	164	
	Fe–P8	1	3.34	0.018	144	

[a]O_w represents the oxygen neighbour associated with water molecules. [b]O_b represents the oxygen neighbour bridging Fe(III) and P(V) centres.

with the associated Fourier transforms (FT's) are shown in Fig. 4(d) and 4(e). A model of the local structure derived from the analysis of the P K-edge and Fe K-edge EXAFS data are shown in Fig. 4(c) and 4(f), respectively. The local structure of this $FePO_4{\cdot}2H_2O$ species is determined to be a tetrahedrally coordinated P^{5+} ion and the Fe^{3+} ions are linked to four bridging (phosphorous atoms) oxygen atoms and two water molecules resulting in a slightly distorted octahedral coordination similar to the one present in the metastrengite structure. Both the Fe K-edge EXAFS and the associated FT's for the iron phosphate catalysts prepared by other methods were found to be very similar to that of the one synthesised by the hydrothermal procedure and the local structural arrangements were determined to be very similar to that shown in Fig. 4(f).

Dynamic measurements

In order to follow the structural modifications that occurred during catalyst calcination to produce an active catalyst we carried out *in situ* combined XRD/QuEXAFS in order for us to be able to follow changes in both long and short range ordering. In Fig. 5 we show the stacked plot of the XRD data recorded using the combined XRD/QuEXAFS measurement procedure during the activation process of the as-prepared iron phosphate catalyst (prepared by hydrothermal methods) between room temperature and 600 °C. We found that the XRD pattern underwent considerable changes during the activation process (see Fig. 5(a)). In Fig. 5(b) we show the variation in the intensity of non-overlapping intense reflections appearing at 2θ angles of 36.39, 23.11 and 29.43°, which represent the as-prepared, tridymite and quartz phases, respectively, of the iron phosphate catalyst. It is clear from Fig. 5(a) and 5(b) that the reflections associated with the as-prepared material appeared to remain intact until the temperature reached *ca.* 150 °C and above which new reflection starts to appear at the expense of those present in the starting material. The loss of reflections of the starting material and the appearance of new reflections were almost instantaneous. These new reflections have been identified as being due to the formation of a tridymite type phase. Although there is no crystallographic information available for the tridymite phase of $FePO_4$, this phase was identified based on the $AlPO_4$ analogue of the tridymite phase.[40,41] The only change in reflections in the XRD pattern recorded between *ca.* 150 °C and *ca.* 500 °C is the increase in intensity and decrease in full-width at half maximum (FWHM) of the reflections corresponding to the tridymite phase. The FWHM extracted from the reflection

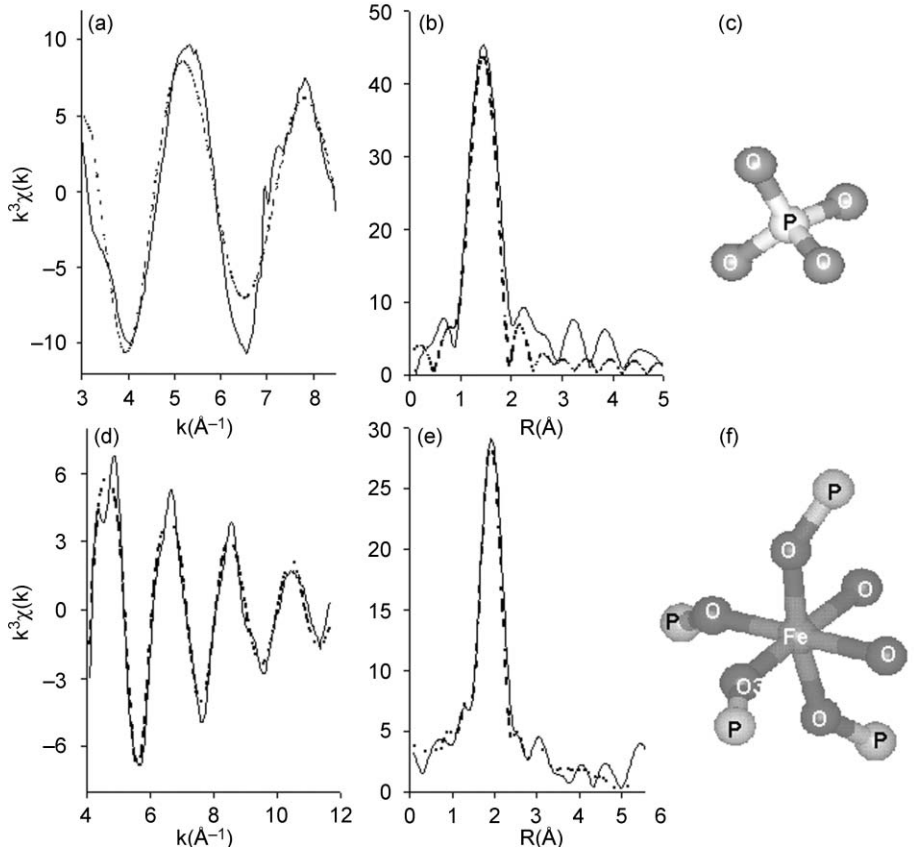

Fig. 4 Best fit between experimental (a) P K-edge EXAFS data and the calculated EXAFS and (b) the associated FT's of the as-prepared iron phosphate catalyst prepared by the hydrothermal method. In (c) we show the local structural model derived from the analysis of the P K-edge data. In (d) and (e) we show the best fit between Fe K-edge experimental and calculated EXAFS and their associated FT's for the catalyst prepared by the hydrothermal method. The solid line and the dashed curve represent the experimental and calculated data, respectively. The local structural model derived by employing the MS analysis procedure is given in (f).

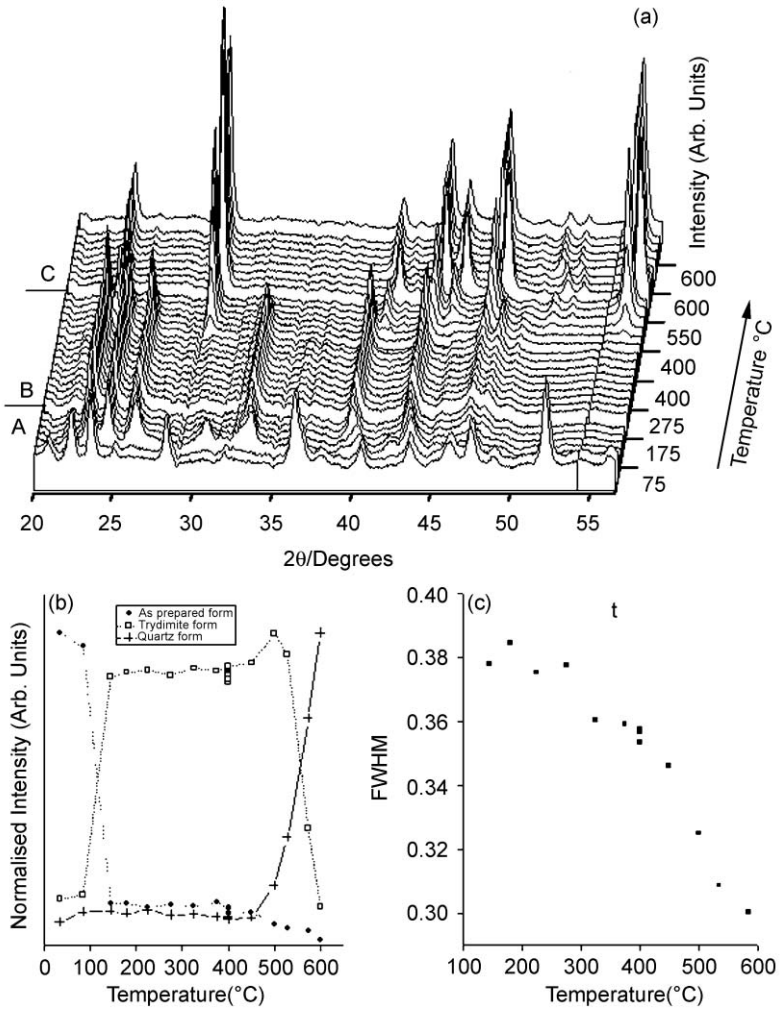

Fig. 5 (a) Stacked XRD patterns of the hydrothermally prepared iron phosphate material recorded during calcination in air from room temperature to 600 °C. The data were collected employing the combined XRD/QuEXAFS method and the patterns were collected below the Fe K-edge, at $\lambda = 1.775$Å. Regions A, B and C correspond to the as-prepared, tridymite and quartz phases, respectively. (b) Variation in the intensities of the reflections appear at 2θ values of 36.39, 23.11, and 29.43°, which represent as-prepared, tridymite and quartz phases of iron phosphate material. (c) Variation in the FWHM of the reflection at $2\theta = 24.3°$, which belongs to the tridymite phase, as a function of temperature.

which appeared at a 2θ value of 24.3°, is plotted against temperature in Fig. 5c. This change in FWHM clearly suggests the growth of bigger particles upon calcination at elevated temperatures; we estimate that the particle size of *ca.* 25 nm grows to *ca.* 35 nm (using the well-known Scherrer equation) before the material undergoes further transformation. On reaching *ca.*

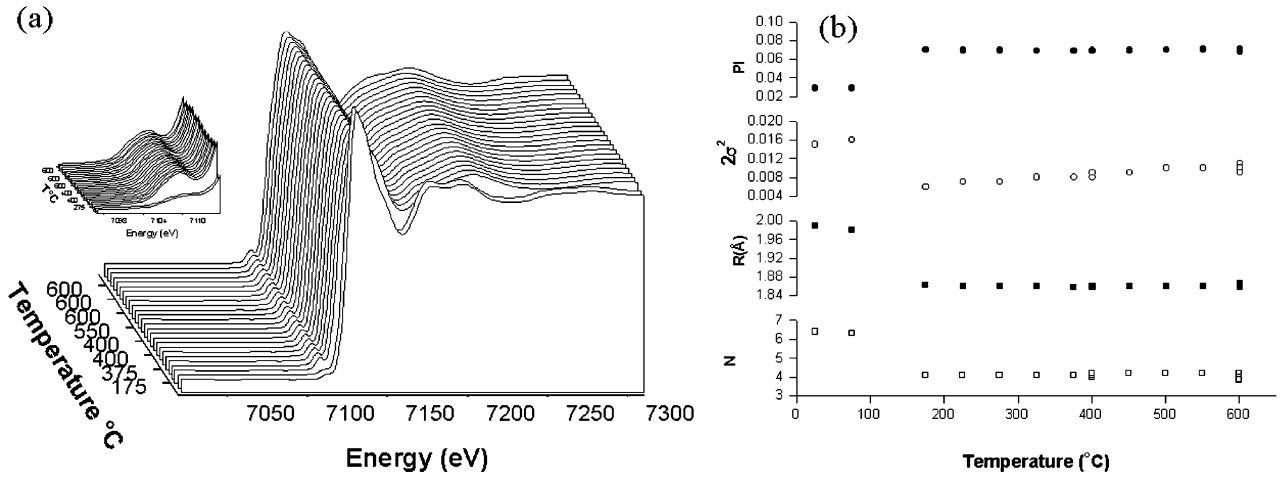

Fig. 6 (a) Stacked plot of the Fe K-edge XAS data recorded during calcination of the hydrothermally prepared iron phosphate, from room temperature to 600 °C. Note that this data set is collected sequentially with the XRD data shown in Fig. 5(a). An expanded region is also given to show clearly the change in the intensity of the pre-edge peak. In (b) we show the variation of pre-edge intensity (PI), coordination number (N), Fe–O distance (R) and $2\sigma^2$ (Debye–Waller factor) with the calcination temperature. The coordination number, Fe–O distance and $2\sigma^2$ were extracted from the analysis of the EXAFS data using single scattering approximation. Note that more than one point appears at 400 °C, which is because the temperature was maintained at 400 °C for 30 minutes before continuing the heating process to 600 °C.

500 °C the well-known phase of $FePO_4$ (quartz type) appears and the transformation from tridymite to the quartz phase was complete at 600 °C (see Fig. 5(b)). No other reflections were detected other than those that belonged to the stoichiometric phases despite the inclusion of excess phosphorus during the initial stages of the synthesis.

Close inspection of the stacked XAS data in Fig. 6(a) clearly indicated that a change in both the XANES and EXAFS data took place when the calcination temperature exceeded *ca.* 150 °C. In particular, in the XANES region an abrupt increase in the intensity of the pre-edge peak, a decrease in the white line intensity and a shift in the frequency of the EXAFS oscillations can be seen. Analyses of the EXAFS data obtained from the dynamic measurement were performed by considring a simple average local structural arrangement of oxygen atoms around the iron as the first neighbours to determine the change in local structural parameters with temperature. In Fig. 6(b) we have plotted the variation in coordination number, average Fe–O distance, Debye–Waller factor (which consists of contributions from static and thermal disorder) and intensity of the pre-edge peak with temperature for the hydrothermally prepared catalyst. The most striking feature seen in the result is the dramatic change that occurs at *ca.* 150 °C. At this point the coordination number, average Fe–O distance and Debye–Waller factor decreased, which coincided with an increase in the XANES pre-edge peak intensity. These changes reflect the formation of a four coordinated Fe^{3+} site. In particular, a decrease in coordination number from *ca.* 6 to 4, a change in Fe–O distance from 1.98 Å to 1.86 Å and an increase in pre-edge intensity is consistent with the XRD observation that the tridymite phase is formed above 150 °C. Note that, like the $AlPO_4$ analogue which is known to contain tetrahedrally coordinated Al^{3+} centers, the $FePO_4$ tridymite phase was seen to contain tetrahedrally coordinated Fe^{3+} centers. On heating above 150 °C only the Debye–Waller factor was seen to increase as a function of temperature; the coordination number, Fe–O distance and the pre-edge intensity remained the same value (within experimental error). This indicated that the local structure remained intact during the process of calcination since both the tridymite and quartz type phases of $FePO_4$ consist of tetrahedrally coordinated iron centers. The changes in the Debye–Waller factors, which consisted of both static and dynamic disorder, can be rationalised as follows. In the initial stages, the octahedral coordination has a large static disorder due to the presence of loosely bound water molecules in addition to the bridging oxygen atoms. Upon removal of the water molecules, a decrease in the Fe–O distances occurred and the change to tetrahedral coordination resulted in an abrupt decrease in the Debye–Waller factor, despite the data being collected at a higher temperature as compared to the as-prepared sample. The subsequent increase in the Debye–Waller factor can be explained as being simply due to an increase in the thermal disorder of the Fe–O pairs present in the tetrahedral arrangement. In order to show the effect of dynamic disorder, we carried out a combined XRD/QuEXAFS measurement of the $FePO_4$ quartz phase at various temperatures using an identical procedure to that of the typical calcination process. As can be seen in Fig. 7, the Debye–Waller factor indeed coincided with that of the data recorded above *ca.* 150 °C.

A more complex picture emerged for the catalysts prepared using the precipitation and ammonia gel methods. Although a plot of the relative intensity of the major reflections (similar to the one shown in Fig. 5(b)) present in the XRD patterns revealed that transformation of the starting material to the $FePO_4$ tridymite and quartz phases occurred between 150 °C and 600 °C (see Fig. 8), similar to that which had been observed for the hydrothermally prepared sample (see Fig. 5(b)), the Fe K-edge XAS results were found to be different. In Fig. 9 we have plotted the variation in the structural parameters, derived from the analysis of the XANES and EXAFS for the catalysts

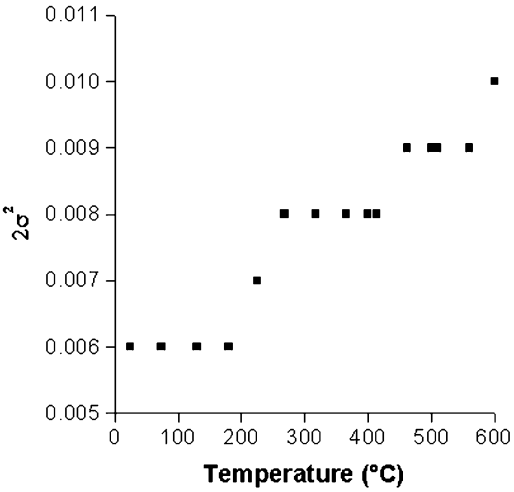

Fig. 7 Variation in $2\sigma^2$ for the $FePO_4$ quartz form with temperature to demonstrate that a systematic increase is seen with an increase in temperature. Note that meaningful data can only be obtained up to three decimal places and hence the scatter in the plot.

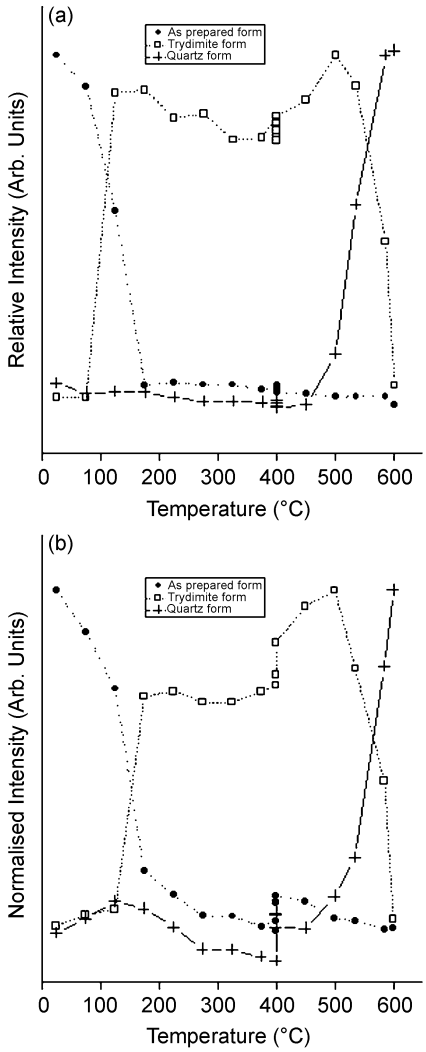

Fig. 8 Variation in the intensities of the reflections that appear at 2θ values of 36.39, 23.11 and 29.43° represent as-prepared, tridymite and quartz phases of iron phosphate material prepared by (a) the precipitation method and (b) the ammonia gel method. The discontinuity and multiple points observed in the data recorded at 400 °C are likely to be due to shrinkage in the sample resulting in the change in the intensity when the temperature was held at 400 °C for 30 minutes.

prepared by precipitation and ammonia gel methods, with temperature. Similar to the observation made for the material prepared by the hydrothermal procedure (see Fig. 6), both these materials underwent a considerable change on reaching *ca.* 150 °C. However beyond 150 °C both catalysts experienced a more gradual decrease in the average Fe–O bond length compared to an abrupt change observed for the hydrothermally prepared material. This slow decrease in Fe–O distance was also seen to coincide with a gradual increase in the XANES pre-edge peak intensity compared to a sharp increase seen for the hydrothermally prepared material. Furthermore for the precipitation catalyst the Debye–Waller factor tended to remain fairly constant with increasing temperature and showed no obvious increase as a direct result of an increase in dynamic disorder (see Fig. 9(a)). For the ammonia gel catalyst slightly different behaviour in the Debye–Waller factor was observed (Fig. 9(b)). Beyond the abrupt fall at *ca.* 150 °C, the Debye–Waller factor was seen to continue to decrease but on exceeding *ca.* 450 °C it was seen to stabilize and remain relatively constant until calcination finished at 600 °C. The final Fe–O average bond length, coordination number, pre-edge peak intensity and Debye–Waller factor values for all three catalyst types at 600 °C are identical to the values found for quartz at the same temperature. This deviation in the behaviour of the these two conventionally prepared materials from that seen for the hydrothermal catalyst is probably due to the presence of small amounts of unknown phase(s) in both the starting materials.

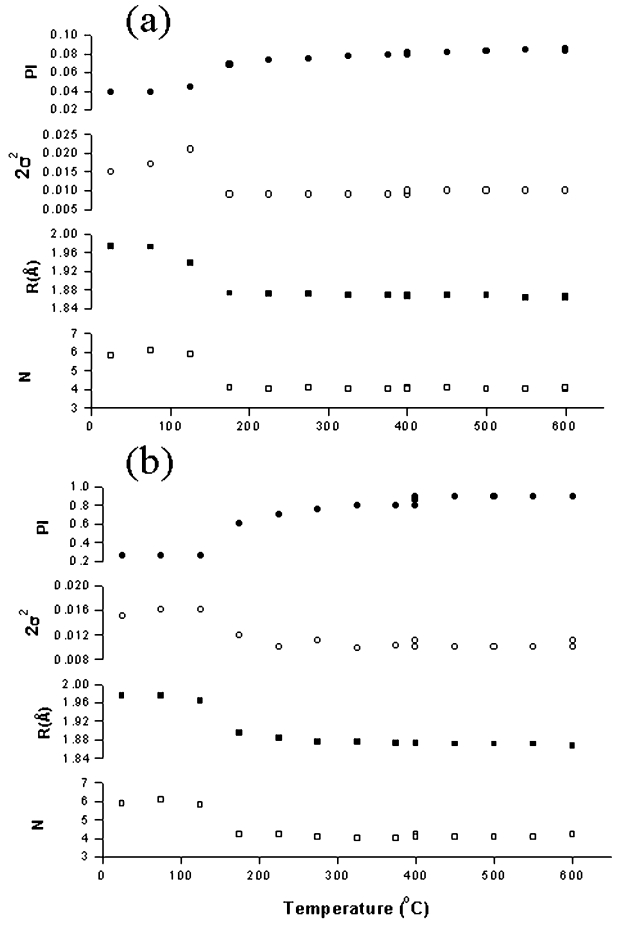

Fig. 9 Variation of pre-edge intensity (PI), coordination number (N), Fe–O distance (R) and $2\sigma^2$ (Debye–Waller factor) with calcination temperature for iron phosphate materials prepared by (a) the precipitation method and (b) the ammonia gel method. The coordination number, Fe–O distance and $2\sigma^2$ were extracted from the analysis of the EXAFS data using single scattering approximation.

Structure of calcined catalysts

Full cluster multiple scattering calculations were also carried out for the calcined catalysts stabilised in either the tridymite or quartz phase. The phosphorus EXAFS results for only the tridymite phase (since the P–O distance in the quartz phase is known) is shown in Fig. 10. Analysis of the data resulted in an average P-O distance of 1.534 Å (see Table 1), which is consistent with a four co-ordinate phosphorus species. The Fe K-edge data was analysed using a similar procedure to that described for the as-prepared catalyst and the only difference for the analysis of this data is the exclusion of the water molecule from the starting model. Structural parameters obtained from the analysis of the Fe K-edge EXAFS data (employing the multiple scattering approach) of the tridymite and quartz structure types formed during calcination of the hydrothermally prepared catalyst are given in Table 2 and the corresponding best fit to the EXAFS and FT's are shown in Fig. 11 along with the local structure arrangements of the Fe^{3+} centers for the tridymite and quartz $FePO_4$ type phases respectively. The results are in complete agreement with the crystallographic data for the $FePO_4$ quartz type phase.[42]

In Table 3 the BET surface area results can be found for the as-prepared catalyst precursors and after calcination at 400 °C and 600 °C respectively. From these measurements it is clear that the hydrothermally prepared iron phosphate catalyst has a larger surface area than the other two catalysts. This initial surface area remains intact for all three catalyst types on calcination to 400 °C but begins to diminish on reaching 600 °C. This reduction in surface area is likely to be associated with the growth in particle size of the tridymite phase before

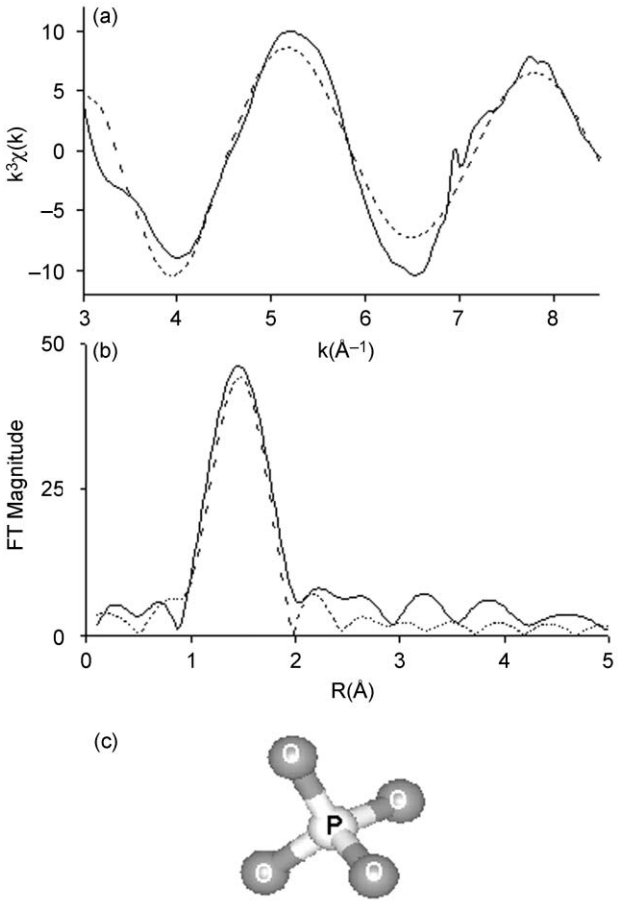

Fig. 10 Typical best fit to the P K-edge EXAFS data of the tridymite phase material and the associated FT's are shown in (a) and (b), respectively. The solid line and the dashed curve represent the experimental and calculated data, respectively. In (c) we show the local structural model around the P(v) ions derived from this best fit.

Table 2 Structural parameters obtained from the analysis of the P K-edge and Fe K-edge EXAFS data of the tridymite and quartz phases of iron phosphate material prepared by heating the hydrothermally synthesised sample

K-Edge	Atom pair	N	R/Å	$2\sigma^2$/Å^2	Fe–O-P angle/°	R factor
P	P–O	3.74	1.534	0.0040		34.61
Fe	Fe–O	4	1.861	0.008		
	Fe–P	1	3.210	0.06	141	
	Fe–P	1	3.193	0.06	129	11.98
	Fe–P	1	3.30	0.06	160	
	Fe–P	1	3.054	0.06	143	
Fe (Quartz)	Fe–O	4	1.857	0.006		
	Fe–P	1	3.164	0.11	139	12.91
	Fe–P	1	3.145	0.11	137	
	Fe–P	1	3.154	0.11	137	
	Fe–P	1	3.145	0.11	136	

transformation to the quartz phase took place. Preliminary catalytic studies for the conversion of isobutyric acid to methacrylic acid employing all the catalysts indeed suggest that the catalyst prepared by the hydrothermal method possesses a higher activity for methacrylic acid production than the catalysts prepared by the conventional methods. A more detailed study

Table 3 Surface area of the catalyst heated at 100 °C (as-synthesised), 400 °C and 600 °C

	Surface area/m^2 g^{-1}		
Preparation method	As-synthesised	Calcined at 400 °C	Calcined at 600 °C
Hydrothermal method	15	14	8
Precipitation method	9	8	4
Ammonia gel method	8	7	4

for both isobutyric acid and lactic acid conversion is currently in progress and will be reported elsewhere.

In summary, all the three synthesis procedures employed here to produce iron phosphate catalyst resulted in the formation of the $FePO_4{\cdot}2H_2O$ type phase in the as-prepared state. In the case of the hydrothermally treated iron phosphate catalyst this was the only phase that formed whereas for the catalysts produced using the precipitation and ammonia gel methods it appears that there are additional (minority) unidentified phases present, which also contain octahedral Fe^{3+} centers. However, irrespective of the method of preparation all these solids are not crystallographically similar to that of metastrengite, a well-known mineral phase of $FePO_4{\cdot}2H_2O$. The detailed *in situ*

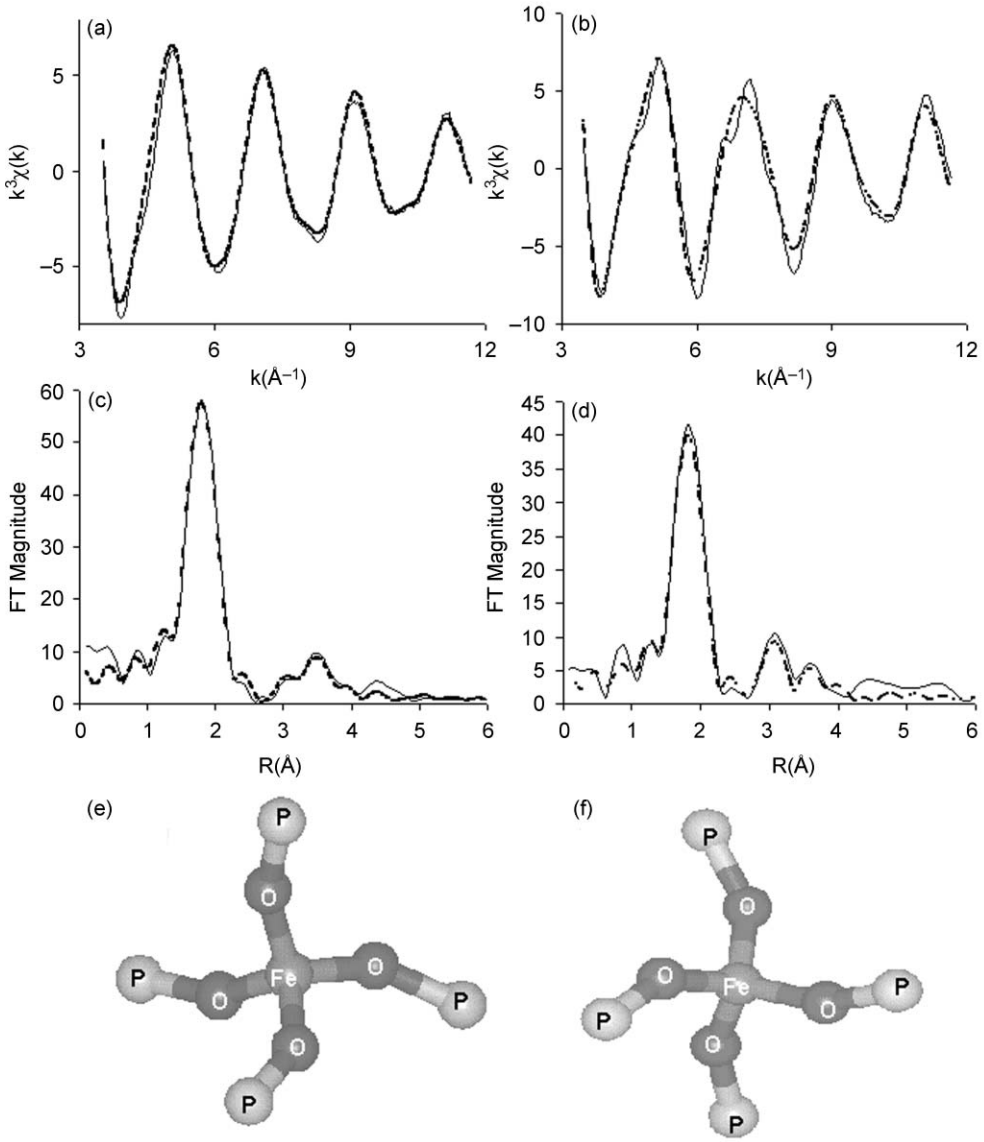

Fig. 11 In (a) and (b) we show the best fit to Fe K-edge EXAFS data of tridymite and quartz phases, respectively, obtained by heating the hydrothermally prepared material. The associated FT's are given in (c) and (d). The solid line and the dashed curve represent the experimental and calculated data, respectively. The local structural models obtained from the final refinement are shown in (e) and (f).

study of iron phosphate catalysts prepared by conventional methods as well as a new approach using hydrothermal techniques, resulted in the formation of the quartz type phase *via* the formation of the tridymite phase and in both these phases iron is present in the 3+ state and in a tetrahedral coordination. Although the phase formations and transformations are found to be very similar, irrespective of the method of preparation, the only differences between them is the presence of small amounts of unknown phase(s) in the catalysts prepared using conventional co-precipitation techniques. This finding of the presence of unknown phases in the conventionally prepared catalysts could have important consequences in the understanding of structure–catalytic property relationships of these materials. But perhaps the most important finding in this investigation is the applicability of hydrothermal synthesis techniques for the preparation of phase pure iron phosphate catalysts in a short period of time, with a surface area higher than that present for the iron phosphate materials produced by conventional methods which may have an effect on catalytic performance.

Acknowledgements

The authors thank EPSRC for financial support and CCLRC for the use of various facilities. AMB would like to thank EPSRC for a quota award and GS thanks the Leverhulme trust for a senior research fellowship. We also thank Miss Christianna Zenonos, Dr David Gleeson, Miss Ilona L. Franklin, Professors C. Richard A. Catlow, Sir John Meurig Thomas, and G. David Price for useful discussions. Use of the ICSD database at CCLRC, Daresbury Laboratory, is gratefully acknowledged. We also thank the ULIRS and in particular Dr Marianne Odlyha for the TGA measurements and Dr Eva Valsami-Jones for surface area measurements.

References

1 J. M. M. Millet and J. C. Vedrine, *Topics Catal.*, 2001, **15**, 139.
2 J. M. M. Millet, *Catal. Rev. Sci. Eng.*, 1998, **40**, 1.
3 K. Hsueh-Yan, BP 1 250 749, 1971.
4 M. Ai, E. Muneyama, A. Kunishige and K. Ohdan, *J. Catal.*, 1993, **144**, 632.
5 M. Ai and K. Ohdan, *Appl. Catal., A*, 1999, **180**, 47.
6 P. Bonnet, J. M. M. Millet, C. Leclercq and J. C. Vedrine, *J. Catal.*, 1996, **158**, 128.
7 M. Ai and K. Ohdan, *Appl. Catal., A*, 1997, **165**, 461.
8 E. Muneyama, A. Kunishige, K. Ohdan and M. Ai, *J. Catal.*, 1996, **158**, 378.
9 M. Dekiouk, N. Boisdron, S. Pietrzyk, Y. Barbaux and J. Grimblot, *Appl. Catal., A*, 1992, **90**, 61.
10 C. Virely, M. Forissier, J. M. M. Millet, J. C. Vedrine and D. Huchette, *J. Mol. Catal.*, 1992, **71**, 199.
11 M. Ai, E. Muneyama, A. Kunishige and K. Ohdan, *Catal. Lett.*, 1994, **24**, 355.
12 M. Ai and K. Ohdan, *J. Mol. Catal. A: Chem.*, 2000, **159**, 19.
13 S. H. Feng and R. R. Xu, *Acc. Chem. Res.*, 2001, **34**, 239.
14 G. Q. Xu, B. Liu, S. J. Xu, C. H. Chew, S. J. Chua and L. M. Gana, *J. Phys.Chem. Solids*, 2000, **61**, 829.
15 M. T. Weller and S. E. Dann, *Curr. Opin. Solid State Mater. Sci.*, 1998, **3**, 137.
16 M. S. Whittingham, *Curr. Opin. Solid State Mater. Sci.*, 1996, **1**, 227.
17 A. M. Beale and G. Sankar, manuscript in preparation, 2002.
18 G. Sankar and J. M. Thomas, *Topics Catal.*, 1999, **8**, 1.
19 J. C. J. Bart, *Adv. Catal.*, 1986, **34**, 203.
20 M. Wilke, F. Farges, P. E. Petit, G. E. Brown and F. Martin, *Am. Mineral.*, 2001, **86**, 714.
21 J. M. Thomas and G. Sankar, *Acc. Chem. Res.*, 2001, **34**, 571.
22 G. Sankar, J. M. Thomas, C. R. A. Catlow, C. M. Barker, D. Gleeson and N. Kaltsoyannis, *J. Phys. Chem. B*, 2001, **105**, 9028.
23 G. Sankar, J. M. Thomas and C. R. A. Catlow, *Topics Catal.*, 2000, **10**, 255.
24 B. S. Clausen, H. Topsoe and R. Frahm, *Adv. Catal.*, 1998, **42**, 315.
25 B. S. Clausen, *Catal. Today*, 1998, **39**, 293.
26 L. M. Colyer, G. N. Greaves, S. W. Carr and K. K. Fox, *J. Phys. Chem. B*, 1997, **101**, 10105.
27 S. R. Davis, A. V. Chadwick and J. P. Wright, *J. Phys. Chem. B*, 1997, **101**, 9901.
28 P. A. Barrett, G. Sankar, C. R. A. Catlow and J. M. Thomas, *J. Phys. . Chem. Solids*, 1995, **56**, 1395.
29 C. Aletru, G. N. Greaves and G. Sankar, *J. Phys. Chem. B*, 1999, **103**, 4147.
30 C. Aletru, G. N. Greaves, G. Sankar and V. Kempson, *Jpn. J. . Appl. Phys., Part 1*, 1999, **38**, 97.
31 G. Sankar, P. A. Wright, S. Natarajan, J. M. Thomas, G. N. Greaves, A. J. Dent, B. R. Dobson, C. A. Ramsdale and R. H. Jones, *J. Phys. Chem.*, 1993, **97**, 9550.
32 J. M. Thomas, G. N. Greaves, G. Sankar, P. A. Wright, J. S. Chen, A. J. Dent and L. Marchese, *Angew. Chem.,-Int. Edn. Engl.*, 1994, **33**, 1871.
33 N. Aliouane, T. Badeche, Y. Gagou, E. Nigrelli and P. Saint-Gregoire, *Ferroelectrics*, 2000, **241**, 1899.
34 E. Pierri, D. Tsamouras and E. Dalas, *J. Cryst. Growth*, 2000, **213**, 93.
35 F. Farges, G. E. Brown and J. J. Rehr, *Geochim. Cosmochim. Acta*, 1996, **60**, 3023.
36 F. Farges, *J. Non-Cryst. Solids*, 1999, **244**, 25.
37 M. Nabavi, F. Taulelle, C. Sanchez and M. Verdaguer, *J. Phys. Chem. Solids*, 1990, **51**, 1375.
38 J. Wong, F. W. Lytle, R. P. Messmer and D. H. Maylotte, *Phys. Rev. B*, 1984, **30**, 5596.
39 D. Gleeson, G. Sankar, C. R. A. Catlow, J. M. Thomas, G. Spano, S. Bordiga, A. Zecchina and C. Lamberti, *Phys. Chem. Chem. Phys.*, 2000, **2**, 4812.
40 H. Graetsch, *Acta Crystallogr., Sect. C: Cryst. Struct. Commun.*, 2000, **56**, 401.
41 H. A. Graetsch, *Acta Crystallogr., Sect. C: Cryst. Struct. Commun.*, 2001, **57**, 665.
42 G. J. Long, A. K. Cheetham and P. D. Battle, *Inorg. Chem.*, 1983, **22**, 3012.